Supplement of Atmos. Meas. Tech., 16, 373–386, 2023
https://doi.org/10.5194/amt-16-373-2023-supplement

Atmospheric Measurement Techniques
Open Access

Supplement of

Electrochemical sensors on board a Zeppelin NT: in-flight evaluation of low-cost trace gas measurements

Tobias Schuldt et al.

Correspondence to: Tobias Schuldt (t.schuldt@fz-juelich.de) and Georgios I. Gkatzelis (g.gkatzelis@fz-juelich.de)

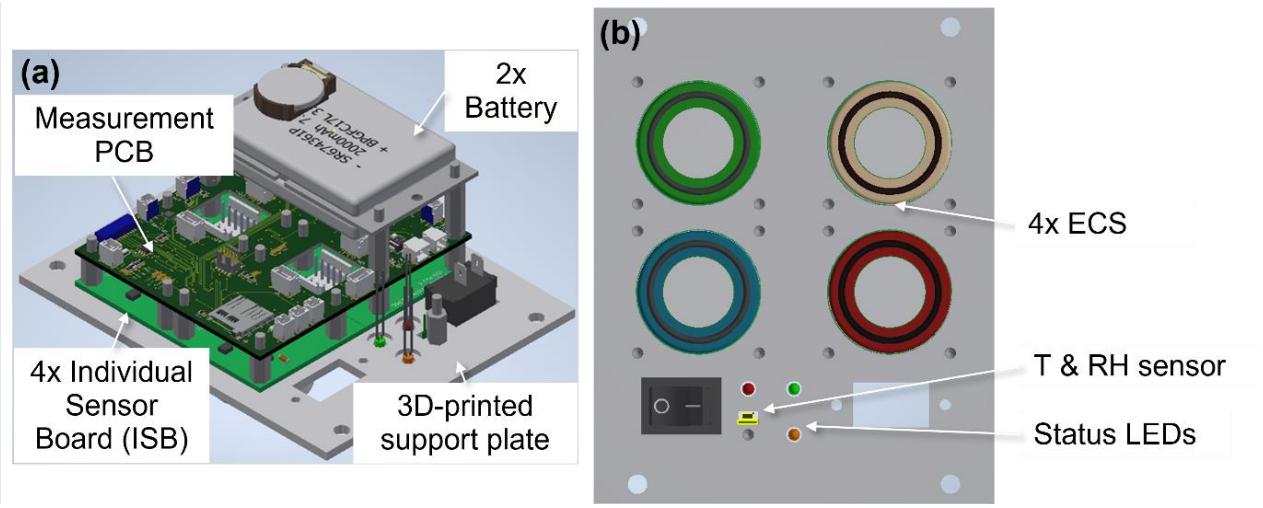

Figure S1: (a) Electronical and mechanical components of the sensor setup we currently use. It is slightly modified, mainly for weight and space reasons, compared to what was used for this study, but the functionality is the same. (b) Bottom view of the setup. PCB: printed circuit board; ECS: electrochemical sensor; T & RH: temperature and relative humidity.

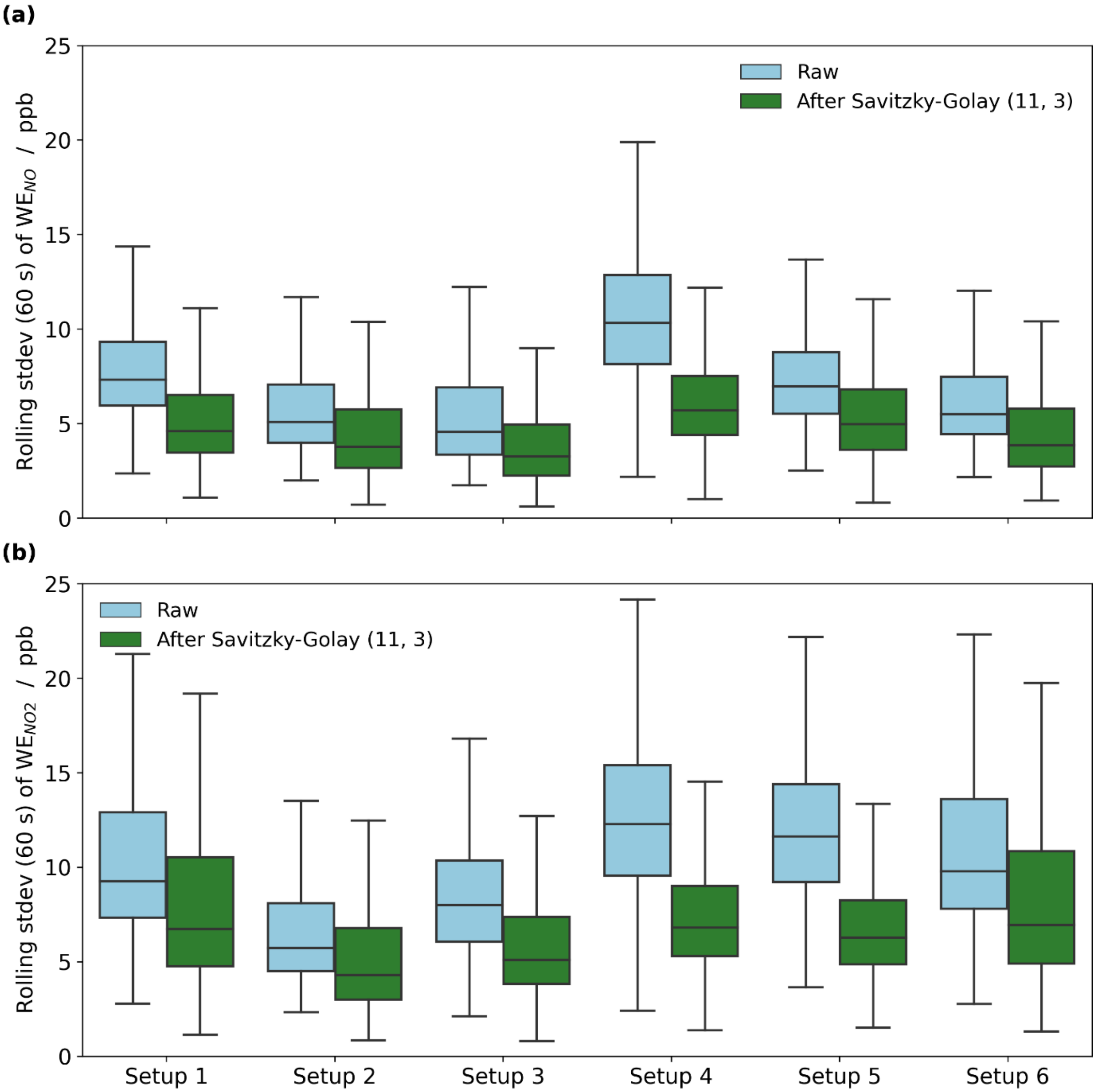

Figure S2: Box and Whisker plots of the rolling standard deviations in 60 s windows for (a) NO and (b) NO_2 of all setups before and after applying a Savitzky-Golay filter with an 11 s window size and a polynomial degree of 3 (see Sect. 2.3.1). Data with > 2 ppb (MIRO) was excluded to evaluate the background noise and reduce influences of peaks on the standard deviation calculations.

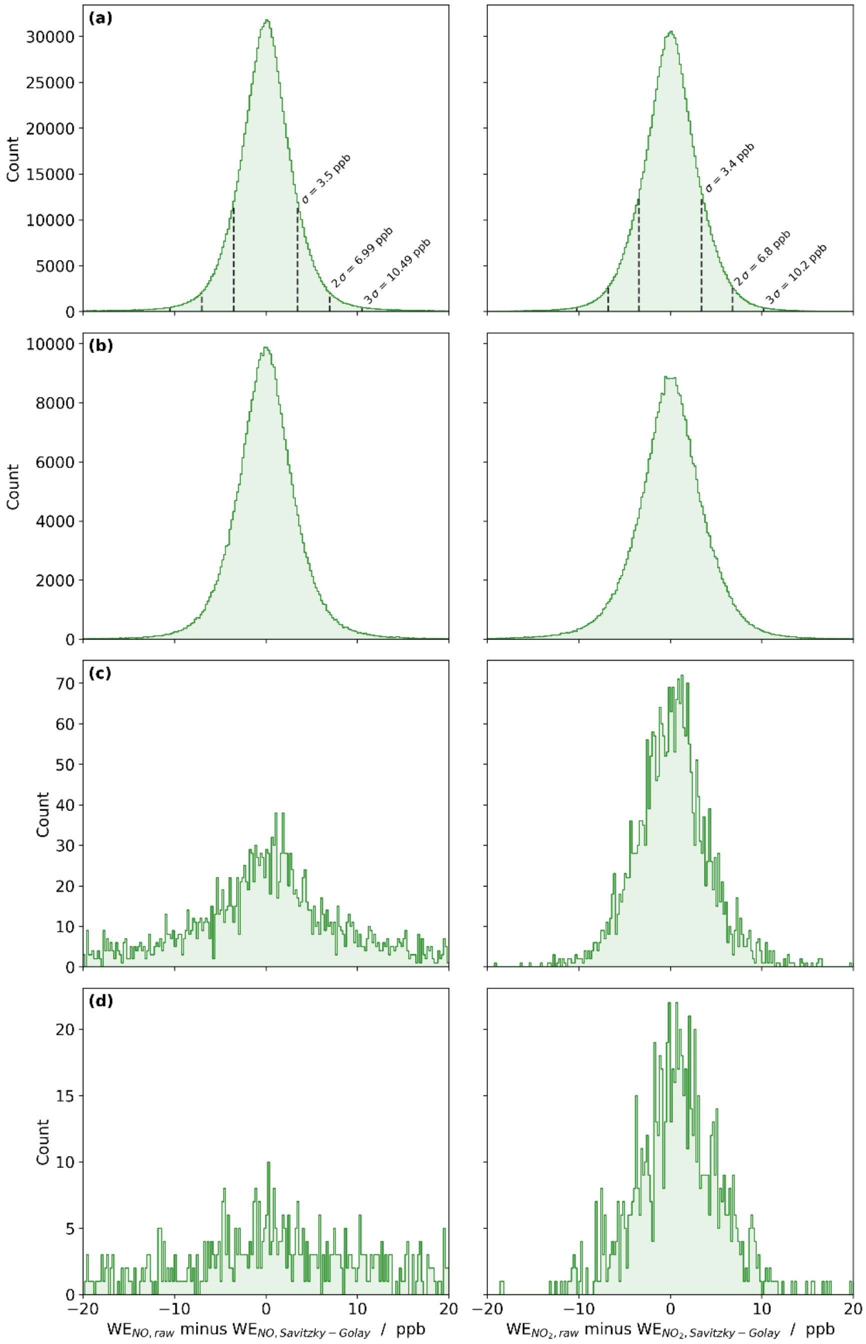

Figure S3: Histograms (setup #2; left: NO, right: NO_2) of the differences between the raw signal and the signal after applying the Savitzky-Golay filter, converted from mV to ppb using the sensors sensitivity. Measurements are binned based on the MIRO instrument to (a) the full data set, (b) measurements below 20 ppb, (c) between 20 ppb and 40 ppb, and (d) above 40 ppb. Dashed lines in (a) indicate multiples of the standard deviations n×σ (n=1, 2, 3). The Savitzky-Golay filters reduction is in the range of 0 to ± 7 ppb for around 95 % (2 σ) of the data, which is within the noise levels given in Fig. S2.

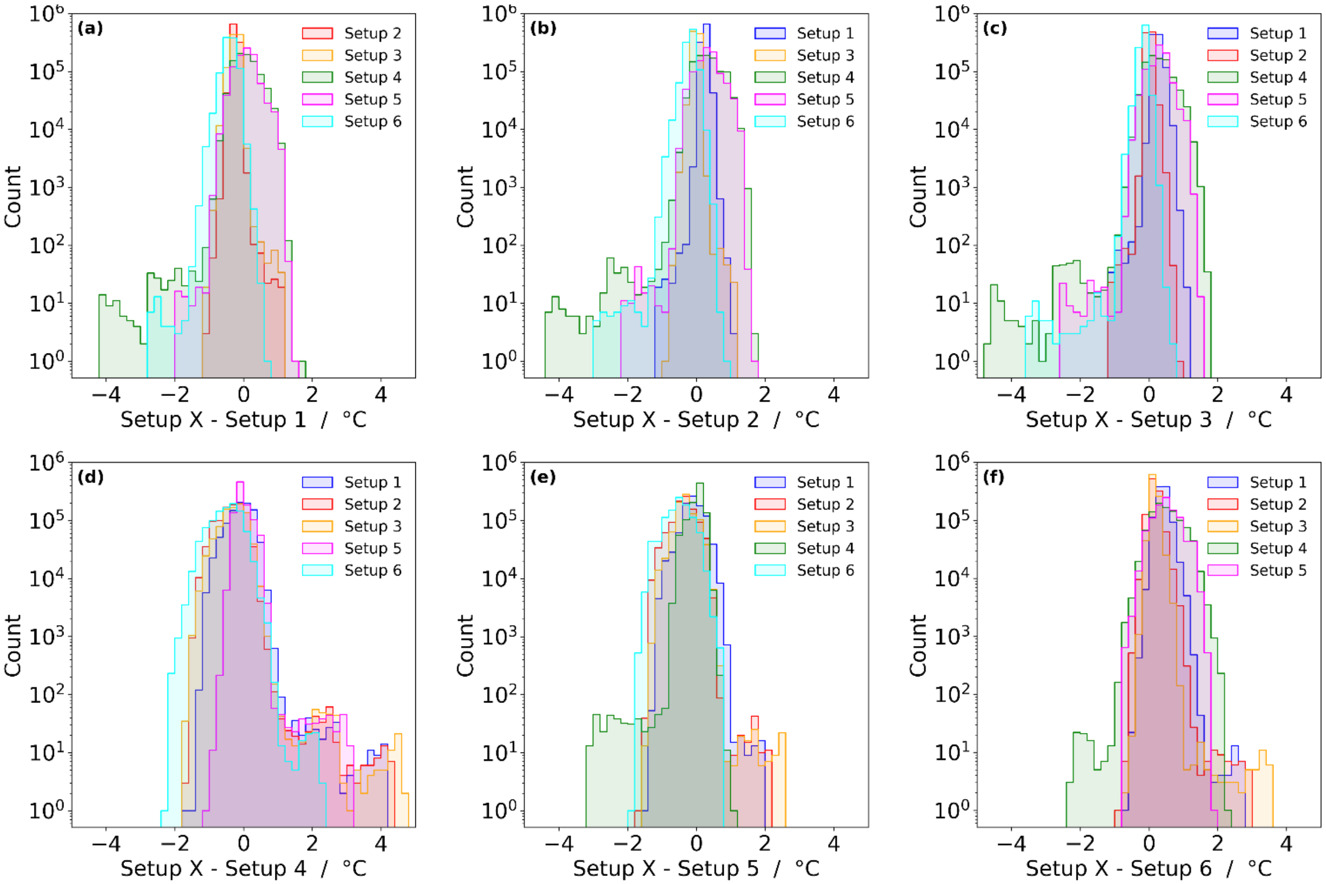

Figure S4: Temperature differences of setup X minus Y, where Y is setup #1 to #6 for (a) to (f), and X is each of the other setups for every plot. Setups #1 to #3 agree well with histogram maxima at around 0. Differences with setups #4 (d) and #6 (f) are shifted more to positive values while setup #5 (magenta) shows broader distributions in comparison to setups #1 to #3.

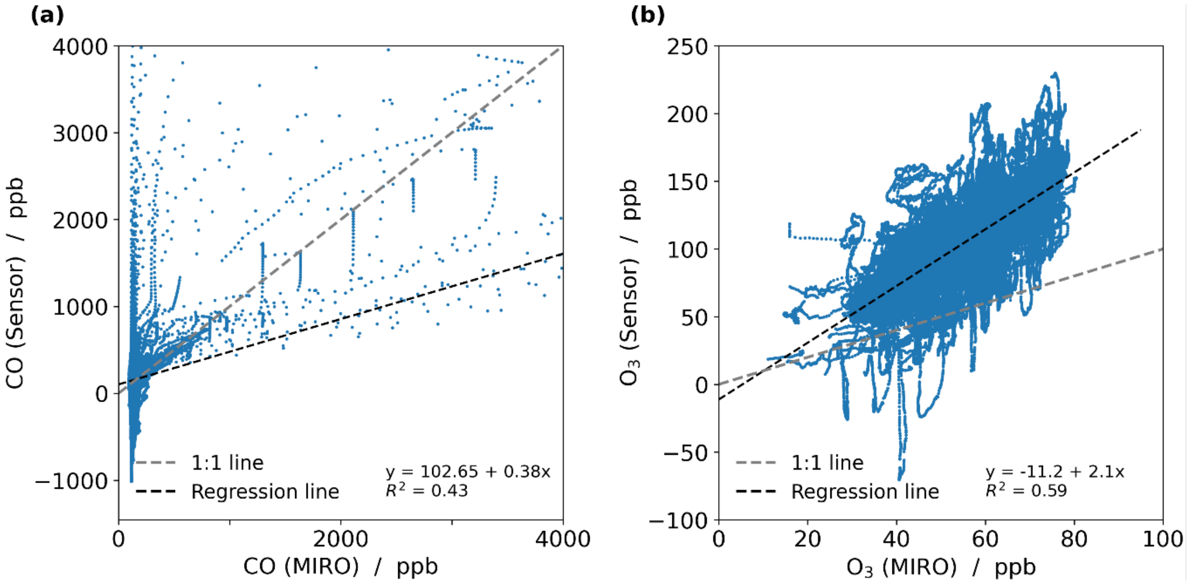

Figure S5: Corrected sensor data with the suggested algorithms from the manufacturer compared to MIRO data for (a) CO and (b) O_3. To use the algorithm, the voltage output for O_3, WE_{O3}, is needed. It is obtained via subtraction of the NO_2 signal from the total Ox sensor output, WE_{Ox}. The NO_2 concentration is determined with the NO_2 sensor on the setup. Equation to obtain the O_3 voltage output: $WE_{O3} = WE_{Ox} - S_{Ox} \times x_{NO2}$ with the sensitivity of the Ox sensor, S_{Ox}, and the NO_2 amount fraction, x_{NO2}.

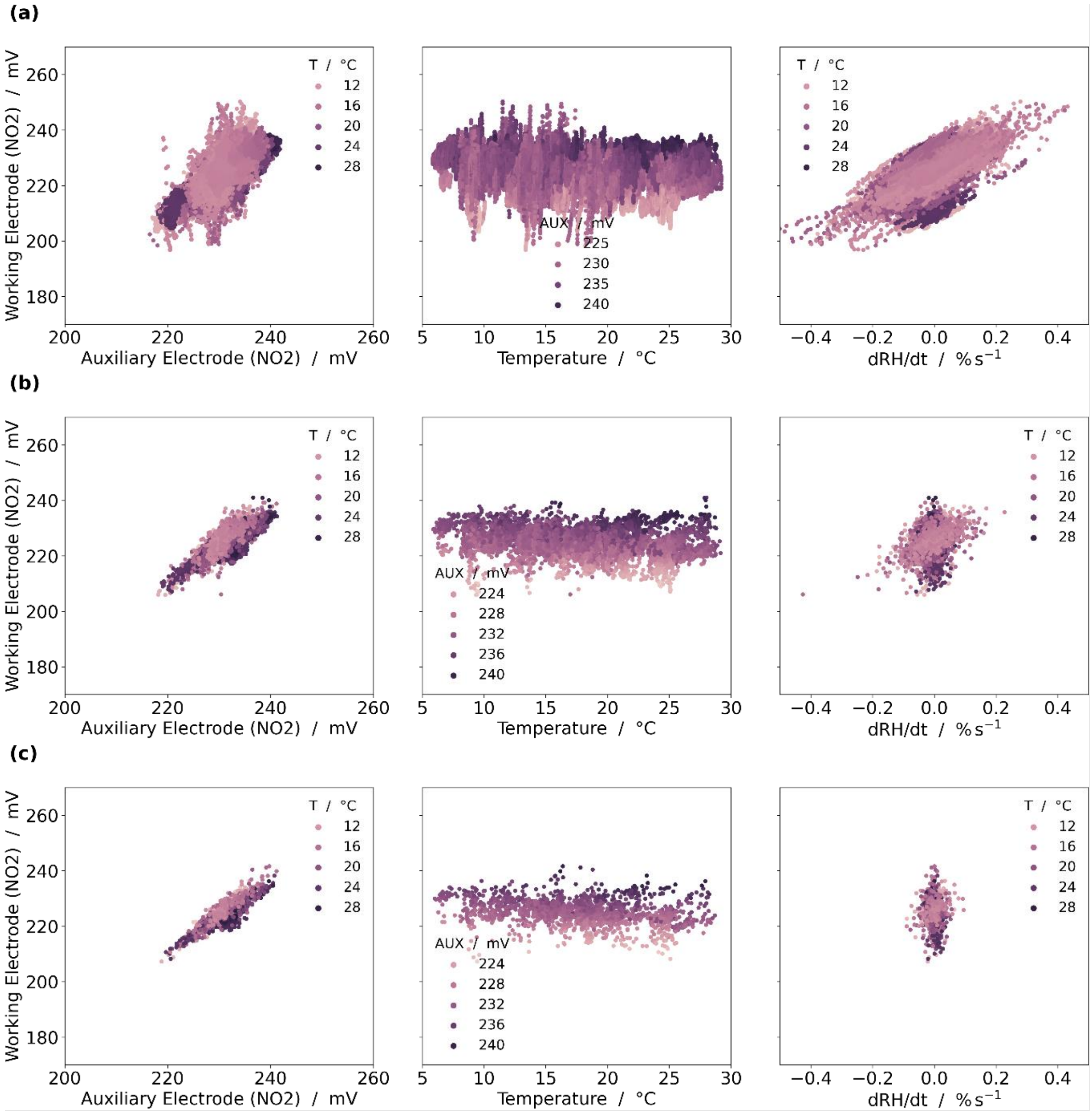

Figure S6: Scatterplots of NO_2 sensor (setup #2) for WE vs. AUX, T and dRH/dt with different time resolutions of (a) 1 s, (b) 30 s and (c) 120 s provided per row.

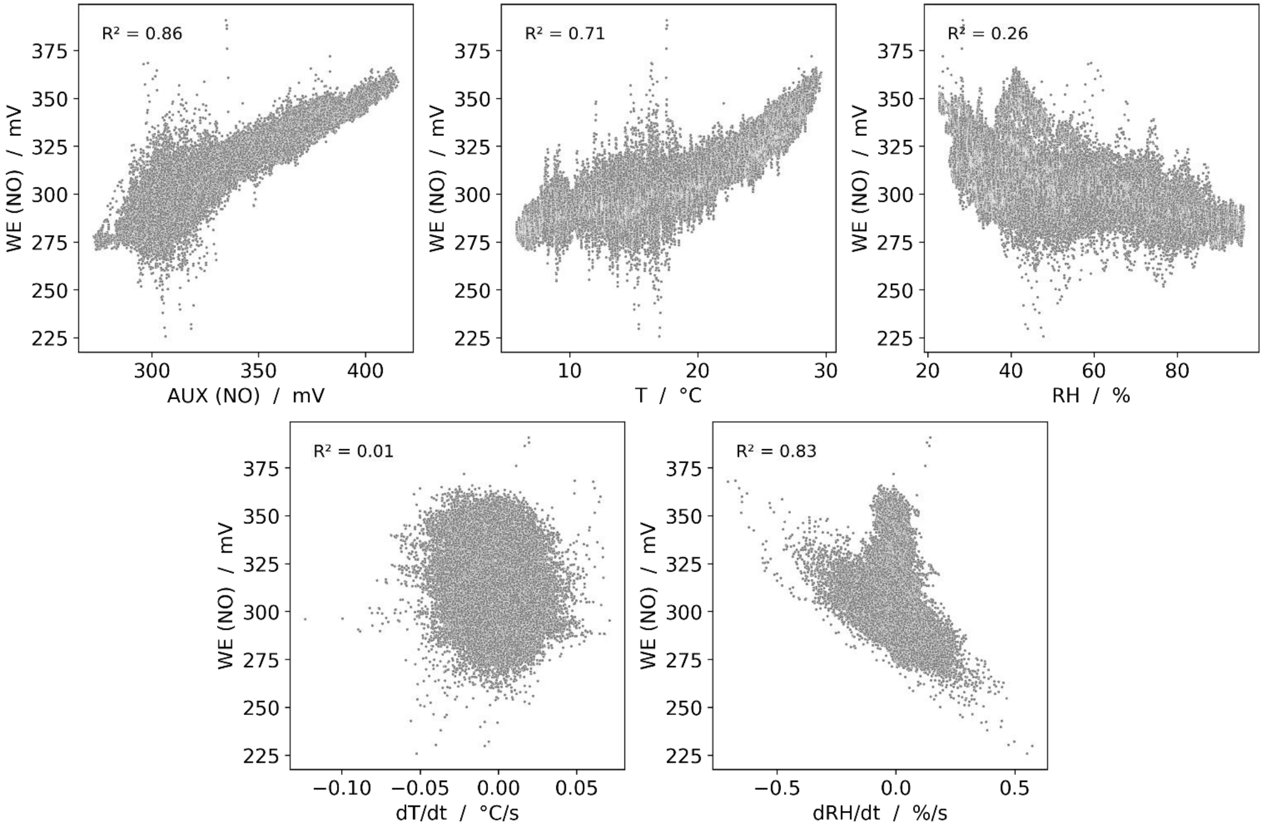

Figure S7: Scatterplots of setup #2's NO working electrode *WE* vs. other possible interferences (auxiliary electrode *AUX*, temperature *T*, relative humidity *RH* and the gradients of *T* and *RH*). *AUX*, *T* and d*RH*/d*t* are used for the correction described in the main text due to their high R^2 of 0.86, 0.71 and 0.83, respectively.

40

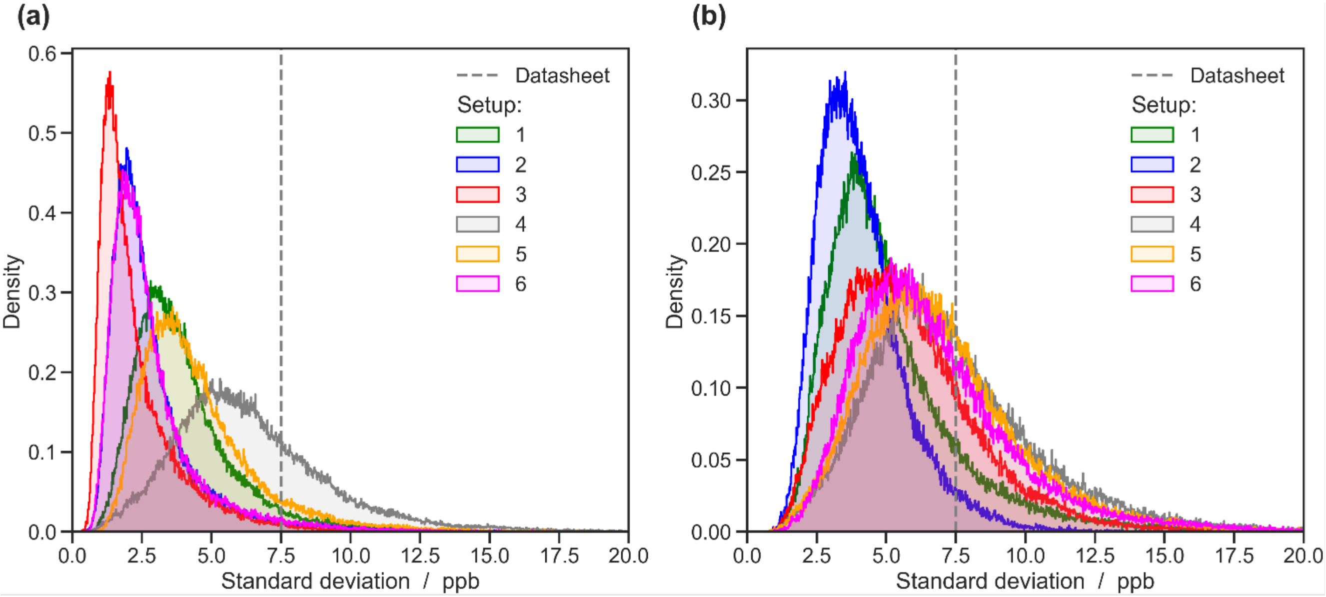

Figure S8: Density distributions of the rolling standard deviations in 31 s windows for (a) NO and (b) NO_2 sensors. This represents the noise of the sensors. The colors correspond to the different sensor setups and the dashed line highlights the data sheet specification of 7.5 ppb (1 σ).

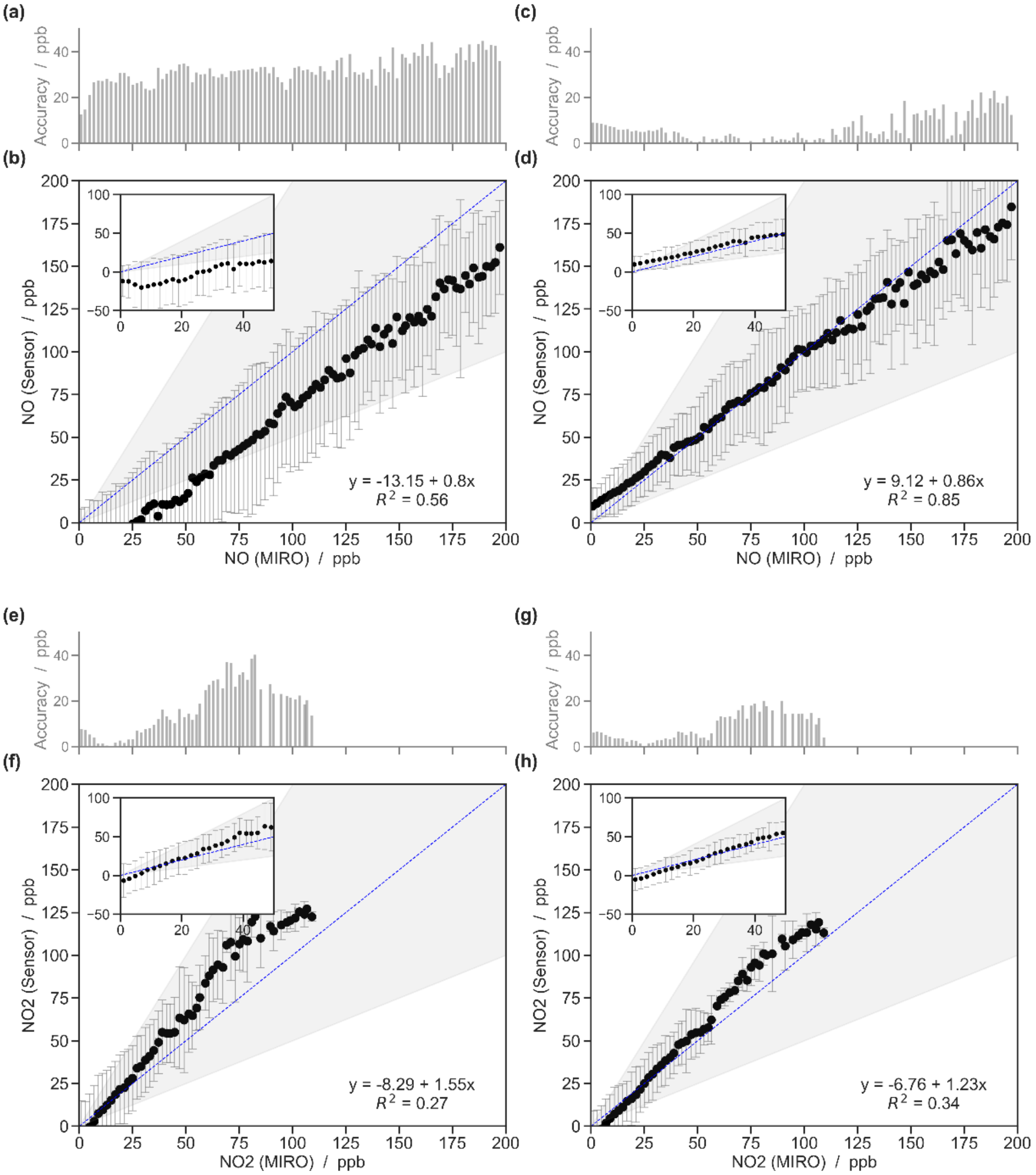

Figure S9: Scatterplots ((b), (d), (f), (h)) of the corrected sensor data of setup #2 (top: NO, bottom: NO_2) vs. MIRO MGA (reference) data classified in 2 ppb bins and two times the standard deviations (± 2σ). On top of the scatterplots the accuracies, i.e., the absolute discrepancies between sensor and MIRO MGA data, for each bin are shown ((a), (c), (e), (g)). Manufacturers correction on the left, our correction method on the right. The dashed blue line marks the 1:1 line and the range of 2:1 and 1:2 is shaded in grey. The inlet plots show the data in a higher resolution from 0 to 50 ppb of the reference instrument. In addition, the linear regression results are shown on the bottom right.

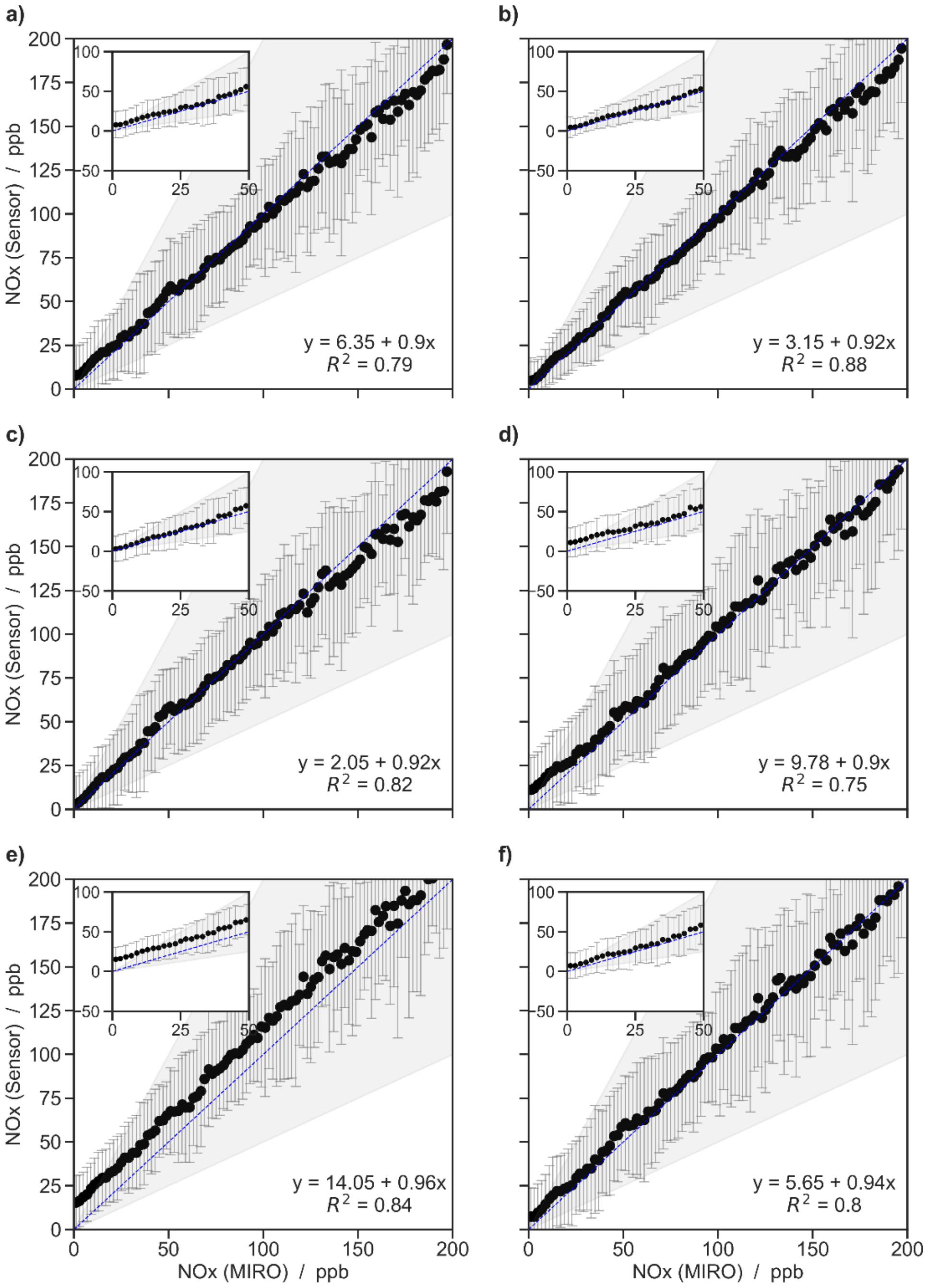

Figure S10: Scatterplots of the corrected sensor data of all setups ((a) to (f) corresponding to setup #1 to #6) vs. MIRO MGA (reference) data classified in 2 ppb bins and two times the standard deviations (± 2σ). The dashed blue line marks the 1:1 line and the range of 2:1 and 1:2 is shaded in grey. The inlet plots show the data in a higher resolution from 0 to 50 ppb of the reference instrument. In addition, the linear regression results are shown on the bottom right. All setups have similar slopes, ranging from 0.90 (a) to 0.96 (e), and intercepts – only setup #5 shows a shift in the positive y direction that is also shown in Fig. 4. Additionally, the R^2 of the linear regressions range from 0.75 (setup #4, (d)) to 0.88 (setup #2, (b)) which is one of the reasons we selected setup #2 for most of the analysis in the main text.

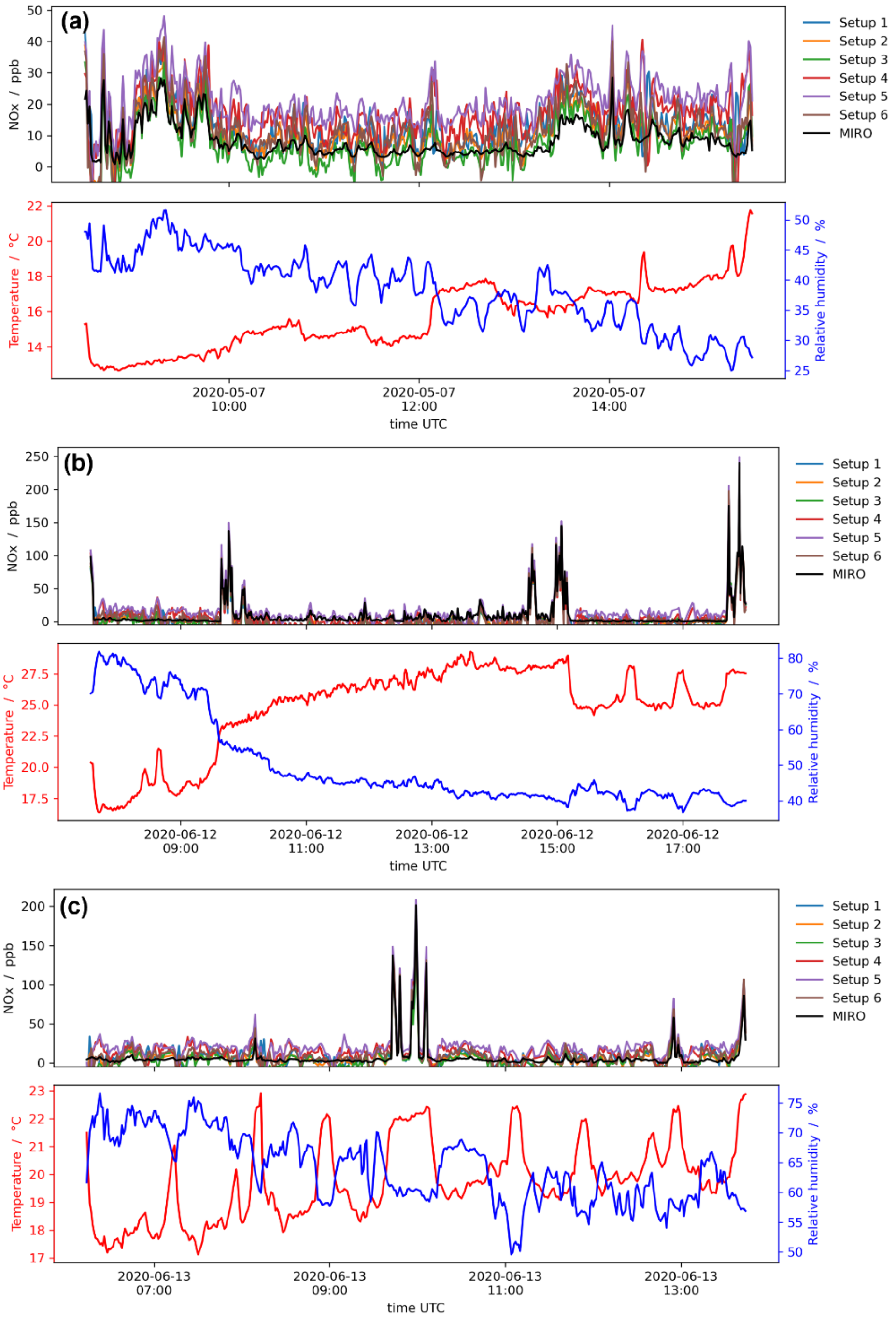

Figure S11: Timeseries of all setups and MIRO MGA for the flight days on (a) 07 May 2020, (b) 12 June 2020, and (c) 13 June 2020. Top: NO_x amount fractions; bottom: *T* and *RH*. The data are averaged to 60 s to reduce the noise and show the trends and stability of the sensors. The temperature fluctuations do not have a significant effect on the amount fractions due to the correction procedure described in this article. There is only an offset from setup #5 to the others that is also reflected by the highest intercept of 14.05 ppb in Fig. S10.

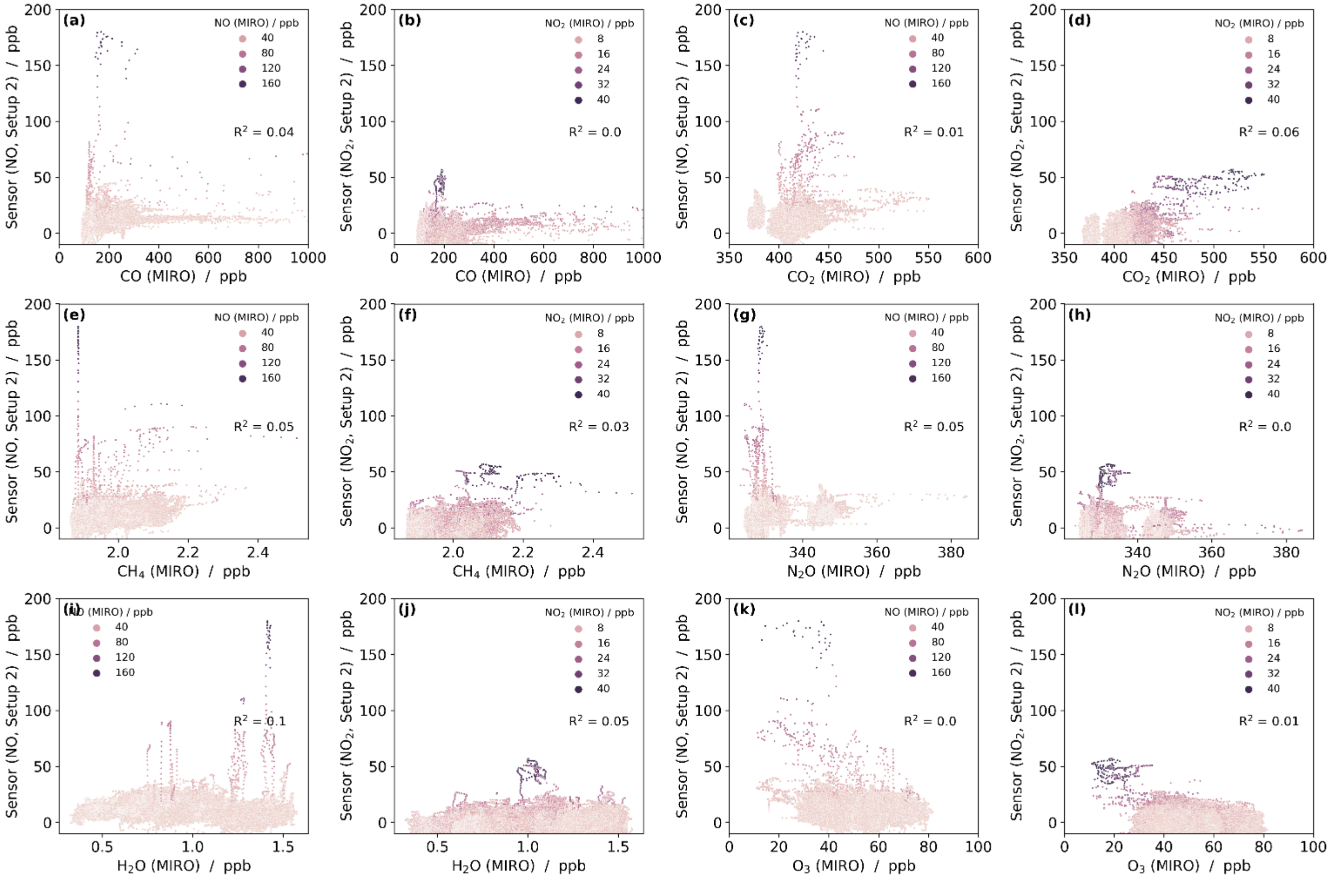

70

Figure S12: Scatterplots of corrected (a, c, e, g, i, k) NO and (b, d, f, h, j, l) NO_2 data for setup #2 versus CO, CO_2, CH_4, N_2O, H_2O, and O_3 measured by the reference device MIRO MGA. There are no significant trends, i.e., cross interferences to the other compounds, also indicated by the R^2.

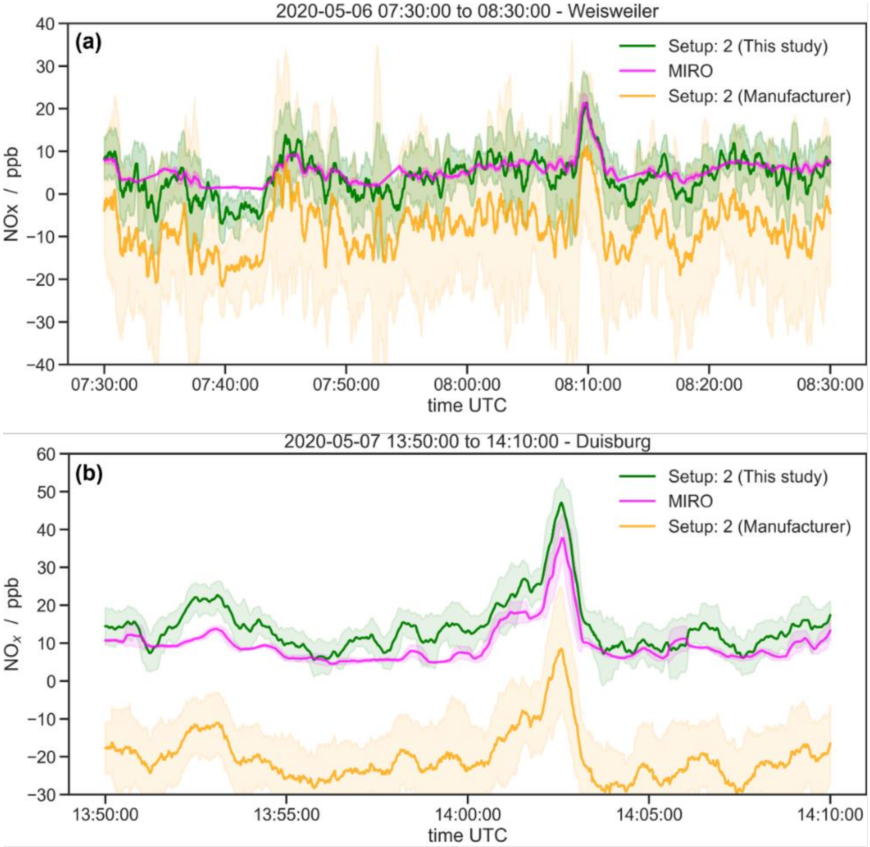

Figure S13: NO$_x$ time series of the flight around Weisweiler (a) and Duisburg (b). Corrected with the algorithms of the manufacturer (orange) and with those developed in this study (green). The shaded areas represent the 1 σ noise of the signals that is significantly reduced after applying the Savitzky-Golay filter and the dRH/dt correction (green time series).

Table S1: Specifications of all sensors provided by the manufacturer. Subscripts of the working electrode (*WE*) and auxiliary electrode (*AUX*) represent zero values (0) and electronic offsets (e).

Analyte	Setup	Sensitivity / mV ppb^{-1}	WE$_0$ / mV	AUX$_0$ / mV	WE$_e$ / mV	AUX$_e$ / mV
CO	1	0.440	411	314	361	322
	2	0.500	429	353	333	341
	3	0.449	441	359	354	344
	4	0.475	430	348	341	346
	5	0.446	422	344	353	348
	6	0.468	400	351	332	355
NO	1	0.580	342	369	276	297
	2	0.573	345	360	279	288
	3	0.540	343	341	286	278
	4	0.580	336	358	275	285
	5	0.526	348	325	282	285
	6	0.560	345	360	285	291
NO2	1	0.254	202	231	213	231
	2	0.269	229	226	228	233
	3	0.247	220	227	221	223
	4	0.268	226	232	231	233
	5	0.266	237	232	239	233
	6	0.239	233	222	239	234
Ox	1	0.252	226	230	232	235
	2	0.253	228	232	231	234
	3	0.281	223	220	226	223
	4	0.271	213	228	221	223
	5	0.274	218	229	223	232
	6	0.231	221	230	222	235

Table S2: Laboratory results of ECS response time t_{90} measurements for NO and NO_2. Amount fraction steps were repeated four times.

Analyte	Amount fractions (step change) / ppb	Response time t_{90} / s
NO	200	35.9 ± 2.9
	300	33.5 ± 0.7
	500	34.3 ± 1.6
	All:	34.6 ± 2.0
NO_2	150	25.8 ± 0.7
	300	29.5 ± 2.3
	600	29.1 ± 1.3
	All:	28.1 ± 1.6

Table S3: Regression parameters to correct for *T, AUX* and d*RH*/d*t*.

Analyte	Setup #	dRH/dt correction	T, AUX correction			
		β_0 / mV $\%^{-1}$ s	α / mV (intercept)	β_1 / mV (T)	β_2 / $°C^{-1}$ (T)	β_3 / - (AUX)
NO	1	-83.53	108.99	2.03	0.09	0.55
	2	-80.25	135.61	1.88	0.09	0.48
	3	-58.44	141.09	1.76	0.08	0.50
	4	-81.15	130.32	0.47	0.13	0.50
	5	-82.50	≈ 0.00	0.31	0.14	0.98
	6	-77.99	139.59	1.39	0.09	0.49
		β_0 / mV $\%^{-1}$ s	α / mV (intercept)	β_1 / $°C^{-1}$ (T)	β_2 / - (AUX)	-
NO_2	1	78.17	-97.06	-0.28	1.36	-
	2	54.48	-64.66	-0.14	1.27	-
	3	47.90	-94.21	-0.13	1.43	-
	4	55.63	-24.17	-0.19	1.10	-
	5	50.10	-4.80	-0.19	1.06	-
	6	74.76	-21.49	-0.17	1.12	-

Correction procedure

Eq. (3) and (4) describe the correction procedure developed in this work that accounts for the *AUX*, temperature and d*RH*/d*t* dependencies of the NO and NO_2 sensors. To numerically correct the *WE* measurements each of these dependencies is separately accounted for by following the above steps.

First, the 1 s time resolution *WE* raw data are plotted vs. d*RH*/d*t* for periods of low analyte concentrations and within changes of ± 0.25 %/s to ± 0.6 %/s, as shown in Fig. S14. A linear correlation is observed and is used to account for the d*RH*/d*t* dependence using the following equation:

$$WE_{dRH/dt}(t) = WE_{raw}(t) - \beta_0 \times \frac{dRH}{dt}(t) \qquad \text{(S1)}$$

In the next step, a modified version of the method developed by Mead et al. (2013) is used to correct the $WE_{dRH/dt}$ for the interference of temperature and possible other influencing factors covered by the auxiliary electrode measurements. Mead et al. (2013) show that a high time resolution (1 s) linear regression analysis of *WE* vs. temperature is challenging due to the longer response times of the ECS which is also evident in this work. Therefore, we use a time window ranging from 60 s up to 600 s gradually shifted over the entire data set. In each window, the minimum of $WE_{dRH/dt}$ and the arithmetic mean values of *T* and *AUX* are determined, respectively. Then the minima $WE_{dRH/dt,min}$ are plotted over the mean *T* and *AUX* and a corresponding function is fitted. The time window that results the highest coefficient of determination is the chosen to describe the fit functions as follows:

$$WE_{NO,T,AUX,dRH/dt}\,(t) = WE_{NO,dRH/dt}\,(t) - \Big(\alpha + \beta_1 \times \exp\big(\beta_2 \times T(t)\big) + \beta_3 \times AUX(t)\Big), \tag{S2}$$

$$WE_{NO_2,T,AUX,dRH/dt}\,(t) = WE_{NO_2,dRH/dt}\,(t)\ - \big(\alpha + \beta_1 \times T(t) + \beta_2 \times AUX(t)\big), \tag{S3}$$

The $WE_{dRH/dt}$ minima are used here to describe periods of low concentrations below the limit of detection of the sensors. This way the observed correlations will reflect the interreferences of the sensors rather than their response to increases of the analyte concentrations. This is a valid approximation for NO and NO_2, since the amount fractions during flights are usually close to 0 ppb and emission peaks tend to be short. However, this method cannot be applied to other gases that have high background concentrations in the troposphere, e.g., ozone and carbon monoxide, given that this background would be subtracted (Popoola et al., 2016).

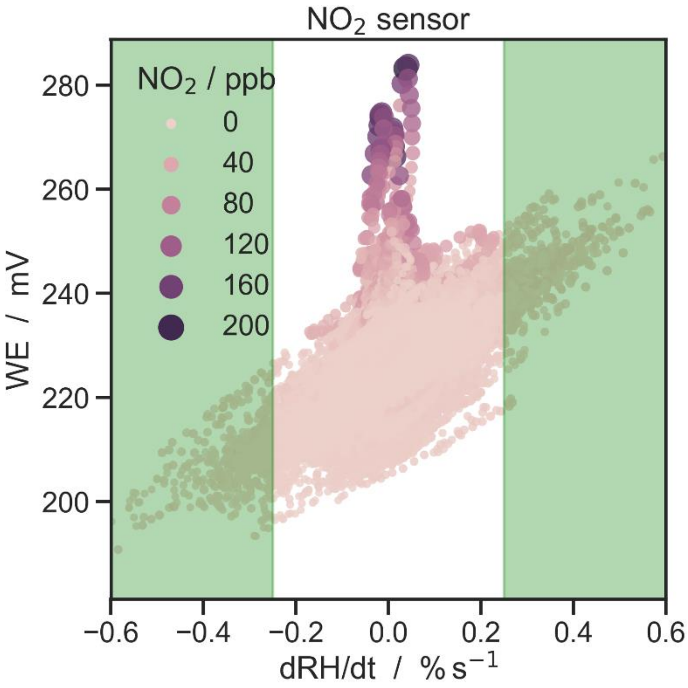

Figure S14: *WE* (NO_2) vs. d*RH*/d*t*, green shaded areas used for regression to mitigate analyte concentration influences on the sensor signal which are mainly found in periods with low values for d*RH*/d*t*.